DNA translocation through a nanopore in a single-layered doped semiconductor membrane

Ining A. Jou, Dmitriy V. Melnikov, Christopher R. McKinney, and Maria E. Gracheva

Phys. Rev. E **86**, 061906 — Published 14 December 2012

DOI: 10.1103/PhysRevE.86.061906

DNA translocation through a nanopore in a single layered doped semiconductor membrane

Ining A. Jou, Dmitriy V. Melnikov, Christopher R. McKinney, and Maria E. Gracheva[1]
Department of Physics, Clarkson University, Potsdam, NY 13699

Recently, we developed a computational model that allows us to study the influence a semiconductor membrane has on a DNA molecule translocating through a nanopore in this membrane. Our model incorporates both the self-consistent Poisson-Nernst-Planck simulations for the electric potential of a solid state membrane immersed in an electrolyte solution together with the Brownian Dynamics of the biomolecule. In this manuscript, we study how the applied electrolyte bias, the semiconductor membrane bias and the semiconductor material type (n-Si or p-Si) affect the translocation dynamics of a single-stranded DNA moving through a nanopore in a single layered semiconductor membrane. We show that the type of semiconductor material used for the membrane has a prominent effect on the biomolecule's translocation time, with DNA exhibiting much longer translocation times through the p-type membrane than through the n-type at the same electrolyte and membrane potentials, while the extension of the biomolecule remains practically unchanged. In addition, we find the optimal combination for membrane/electrolyte system's parameters to achieve longest translocation time and largest DNA extension. With our single layered electrically tunable membranes, the DNA translocation time can be manipulated to have an order of magnitude increase.

I. INTRODUCTION

Nanopores have become a useful tool for identifying and characterizing biomolecules[1]. Of particular interest is the promising use of nanopores in biomolecular sensors and possibility of rapid sequencing of DNA. In this set-up DNA is forced through a nanopore in a membrane via an electric bias across the membrane. The resulting blockage of ionic current can be measured using the resistive-pulse technique, and it's duration and magnitude correlated to specific DNA characteristics such as DNA base composition and length of the biomolecule[2–4].

Nanopores in solid-state membranes were originally developed in the likeness of biological nanopores in lipid bilayer membranes. They addressed some of the drawbacks of bio-nanopores and allowed for versatility in size and function. While biological nanopores have the obvious advantage of being biocompatible to biomolecules, solid-state membranes could be more stable and size-controllable than their biological counterparts[5–7]. In addition, artificial nanopores offer the opportunity of electrical tunability specific to certain biomolecules[8–14]. Through ion- or electron-beam sculpting[15], nanopores can be fabricated in a silicon membrane down to a single nanometer in diameter[7,16]. Thus solid-state nanopores have been increasingly studied to assess their ability to characterize both single-stranded and double-stranded DNA (ssDNA and dsDNA, respectively)[7].

Despite the above advantages of solid-state nanopores for DNA characterization, there are still many issues to be confronted. Currently, the average translocation time per DNA base pair is of the order of $1 - 20$ μs[17,18]. At this timescale, ionic current changes from DNA bases are indistinguishable from ionic current noise and interference from the secondary structure of the translocating molecule[8,19–21]. Therefore, the goal of much of the research is to control the translocation time of the biomolecule, such as increasing the translocation time to allow for longer sampling times for each nucleotide[22,23].

Electrically tunable semiconductor membranes have been studied by us to this effect[9,14,24]. In our solid state membrane devices, the membrane material is a semiconductor, which allows us to apply electric bias to the membrane (or membrane layers), which in turn, affects the electric potential distribution in the pore. Thus, we are able to control the magnitude and the spacial landscape of the electric potential in the nanopore through the use of different semiconductor material parameters, combination of semiconductor layers, as well as application of electric bias to these layers[9,14]. Such versatility allowed us to significantly slow down and even momentarily trap a translocating biomolecule[14].

In this paper, we study semiconductor membranes made of a single layer of silicon (Si). Two material types have been considered, n-type and p-type, both considered materials were highly doped to maximize the tunable range for the electric potential generated by the membrane. The electric bias applied to the membrane is denoted by V_m. We apply electrolyte bias in a regular fashion, above and below the membrane, which is denoted as V_e. This electrolyte bias initiates the biomolecule translocation through the nanopore. We address how the semiconductor material type (n or p), applied membrane and electrolyte biases affect the translocation time and elongation of a ssDNA permeating through a nanopore in a thin membrane. Brownian Dynamics (BD) simulation is used to study DNA motion in an electric potential obtained from the self-consistent solution of the Poisson-Nernst-Planck (PNP) model. We show that ssDNA translocation dynamics is strongly dependent on the type of membrane utilized, with p-Si membranes

[1] Corresponding author: gracheva@clarkson.edu

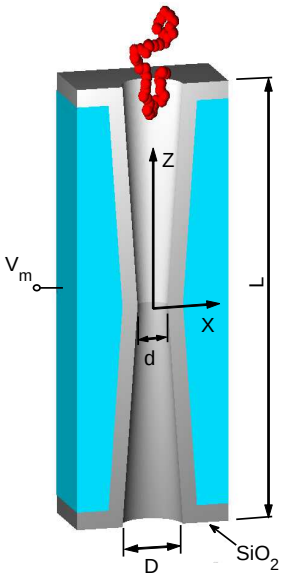

FIG. 1: (Color online) Schematic representation of the modeled doped Si membrane with a double conical nanopore and ssDNA entering it. x- and z-axis originate from the center of the pore. Illustration is not to scale. Membrane thickness is $L = 25$ nm, the inner pore diameter is $d = 2$ nm, and $D = 4$ nm is the outer pore diameter.

showing longer translocation times and biomolecule extensions.

This paper is structured in the following manner. The following section details our PNP-BD approach. In Section III we present DNA translocation simulations for different membrane and electrolyte biases. Section IV concludes with a brief summary of the work.

II. MODEL DESCRIPTION

A. Poisson-Nernst-Plank Model

The modeled membrane, schematically shown in Fig. 1, has a total thickness of $L = 25$ nm and consists of 23 nm of the doped Si (n- or p-Si) and 1 nm layer of SiO_2 at the surface. The nanopore has a double conical shape with inner pore diameter of $d = 2$ nm and outer pore diameter of $D = 4$ nm. The membrane is submerged in an electrolyte solution of KCl with $C_{KCl} = 0.2$ M.

The calculated Debye screening length $L_D = \left[\varepsilon_0 {\varepsilon_r}^{KCl} k_B T/(2e^2 C_{KCl})\right]^{1/2} \sim 0.68$ nm for bulk concentration of $C_{KCl} = 0.2$ M at room temperature, where e is the positive elementary charge. The fact that L_D is smaller than radius of the pore constriction allows the application of the continuum Poisson-Nernst-Plank approach to obtain the electric potential distribution in the membrane and electrolyte[25,26]. This is done by solving Poisson equation,

$$\nabla \cdot [\varepsilon(\mathbf{r}) \nabla \phi(\mathbf{r})] = -\rho(\mathbf{r}), \tag{1}$$

TABLE I: Values of model parameters (with their meaning) utilized in the simulations.

Symbol	Description	Value
${\varepsilon_r}^{SiO_2}$	Relative permittivity of SiO_2	3.9
${\varepsilon_r}^{Si}$	Relative permittivity of Si	11.7
${\varepsilon_r}^{KCl}$	Relative permittivity of KCl	78
N_D	Donor density	2×10^{20} cm^{-3}
N_A	Acceptor density	2×10^{20} cm^{-3}
N_{surf}	Surface charge density	4×10^{20} cm^{-3}
D_{K^+}	Diffusion coefficient	1.95×10^{-5} cm^2/s
D_{Cl^-}	Diffusion coefficient	2.03×10^{-5} cm^2/s
ξ	Solution viscosity	7.5×10^{-9} Ns/m
δt	Time step	5 ps
T	Temperature	300 K
N_b	Number of beads	45
k_{el}	Elastic constant	171 kcal/(mol Å^2)
r_0	Equilibrium bond length	3.4 Å
ϵ_b	Interaction strength	0.1 kcal/mol
σ_b	LJ radius (bead-bead)	6.5 Å
σ_m	LJ radius (bead-membrane)	2.5 Å

in conjunction with the steady-state Nernst-Plank equations[25] to obtain local concentrations of potassium ions, $C_{K^+}(\mathbf{r})$, and chlorine ions, $C_{Cl^+}(\mathbf{r})$,

$$\nabla \cdot [\mu_i C_i \nabla \phi + z_i D_i \nabla C_i] = 0, \qquad i = K^+,\ Cl^-, \tag{2}$$

where μ_i is the mobility of the i-th species, $D_i = \mu_i k_B T/e$, and $z_i = \pm 1$. See Table I for numerical values of all parameters.

The charge density $\rho(\mathbf{r})$ in Eq. (1) has contributions from the charge in electrolyte, $\rho_e(\mathbf{r})$, and in membrane, $\rho_m(\mathbf{r})$, given by

$$\rho_e(\mathbf{r}) = e\left\{C_{K^+}(\mathbf{r}) - C_{Cl^-}(\mathbf{r})\right\} \tag{3}$$

and

$$\begin{aligned}\rho_m(\mathbf{r}) = e\{&p(\mathbf{r}) - n(\mathbf{r}) + N_D(\mathbf{r}) \\ &-N_A(\mathbf{r}) - N_{surf}(\mathbf{r})\},\end{aligned} \tag{4}$$

where $p(\mathbf{r})$ and $n(\mathbf{r})$ are the concentrations of electrons and holes, while $N_D(\mathbf{r})$ and $N_A(\mathbf{r})$ are the donor and acceptor densities in the semiconductor regions[27], with N_D (N_A) being non-zero in the n (p)-type membrane. The dopant charge density values used to generate membranes of n-type and p-type are given in Table I. $N_{surf}(\mathbf{r})$ represents negative surface charge on the membrane (on the SiO_2 layer). The electrons and holes in the semiconductor regions obey Fermi-Dirac statistics[28]. Further details of the model are discussed in previous publications[29–31].

B. Brownian Dynamics Model of DNA

The movement of the ssDNA through the nanopore is described using Brownian Dynamics approach[32–36] with parameters chosen to reproduce properties of a real ssDNA such as a characteristic persistence length, nucleotide charge and size, and distance between nucleotides. The persistent length of the ssDNA is found to be about the length of one nucleotide at high solution concentrations[37], thus, we represent ssDNA molecule as a freely joined chain of beads. In our model each DNA nucleotide is modeled by one bead composed of a phosphate, sugar and a base, and carrying charge $q_i = -1e$. The solution of the discretized Langevin equation, which determines the position of each bead on the biomolecule at a time t, is written as

$$\mathbf{r}_i(t) = \mathbf{r}_i(t-\delta t) - \nabla_i U[\mathbf{r}_i(t-\delta t)]\frac{\delta t}{\xi} + \sqrt{\frac{6\delta t k_B T}{\xi}}\mathbf{n}_i, \quad i = 1 \dots N_b, \tag{5}$$

where the last term is due to the stochastic force. This force is responsible for random movement of beads, with $\mathbf{n}_i$ being the three-dimensional unit vector with components uniformly distributed in the interval $[-1, 1]$. See Table I for numerical values of parameters.

The potential energy $U(\mathbf{r}_i)$ of the i-th bead in Eq. (5) is

$$U(\mathbf{r}_i) = U_{el} + U_b + U_m + U_C + q_i\phi(\mathbf{r}_i). \tag{6}$$

It has the following contributions:

- the elastic bond stretch energy:

$$U_{el} = k_{el}\sum_{j=i\pm1}(r_{ij} - r_0)^2 \tag{7}$$

  where $r_{ij} = |\mathbf{r}_i - \mathbf{r}_j|$, $j = i \pm 1$, is the bond length between the consecutive i-th and j-th beads[32];

- U_b describes the excluded volume effects among the beads due to the short range Lennard-Jones (LJ) interaction energy with $\sigma = \sigma_b$:

$$U_b = \epsilon_b \sum_{j,j\neq i}\left[\left(\frac{\sigma}{r_{ij}}\right)^{12} - 2\left(\frac{\sigma}{r_{ij}}\right)^{6}\right]; \tag{8}$$

- the Lennard-Jones interaction energy between the beads and the membrane surface, U_m, is given by equation similar to Eq. (8) where we replace r_{ij} by the distance between the i-th bead and the nearest point on the membrane surface and take $\sigma = \sigma_m$ ($\sigma_m < \sigma_b$ because beads can be closer to the membrane surface than to each other);

- the screened Coulomb interaction U_C among the charged beads

$$U_C = \frac{1}{4\pi\varepsilon_0{\varepsilon_r}^{KCl}}\sum_{j,j\neq i}\frac{q_i q_j}{r_{ij}}\exp\left[\frac{-r_{ij}}{L_D}\right] \tag{9}$$

  due to the phosphate backbone charges q_i (contributions from small positive charges on bases and sugars are neglected) screened by the ionic charges in the solution;

- the external electric energy $q_i\phi(\mathbf{r}_i)$ with electric potential ϕ calculated from the self-consistent solution of Eqs. (1) - (4).

In our model we did not include bending potential energy of DNA since the persistence length of a ssDNA is found to be about the length of one nucleotide at high solution concentrations[37].

C. Simulation Details

By varying both the electrolyte bias, V_e, and the applied membrane bias, V_m, we study how they affect ssDNA translocation dynamics. To characterize ssDNA behavior during translocation, we record the biomolecule translocation time (dwell time) through a nanopore as $\tau = t_{out} - t_{in}$. Here $t_{out(in)}$ is the time when the center of mass of the ssDNA exits (enters) the pore. The gyration radius $R_g = [(2N_b^2)^{-1}\sum_{ij} r_{ij}^2]^{1/2}$ is also calculated to track the biomolecule extension during the translocation process.

Since the movement of the biomolecule through the pore is stochastic in nature, for each (V_e, V_m) combination, 10^3 BD simulations were performed at 100 million time steps each. The simulations were carried out as follows. First, the electric potential distribution in the system is calculated using the PNP model. The biomolecule is generated and then relaxed for 0.125 ms (25 million time steps) in the absence of the membrane and external potential, thus a free floating ssDNA, to achieve a realistic randomly positioned biomolecule. Equilibrium gyration radius for our ssDNA is R_g~15 Å. The relaxed biomolecule is placed near the opening of the nanopore (distance between the center of mass position of the relaxed polymer and the pore's opening is 10 Å), and its subsequent movement is tracked and analyzed.

III. RESULTS AND DISCUSSION

A. Zero Membrane Bias: $V_m = 0$

In this Section we focus on how the translocation of a ssDNA through a pore in n-Si and p-Si membrane is affected by electrolyte bias V_e with no applied membrane bias: $V_m = 0$. We vary the electrolyte biases in the interval 0.15 V$\leq V_e \leq$ 0.8 V. Looking at the electric potential profiles along the z-direction (pore axis, see Fig. 1), in Fig. 2a we note a monotonic variation of ϕ from the positive coordinates (nanopore entrance at z=120Å) to the negative coordinates (nanopore exit at z=-120Å) along the z-direction. This is predominantly due to the applied electrolyte bias, which also initiates

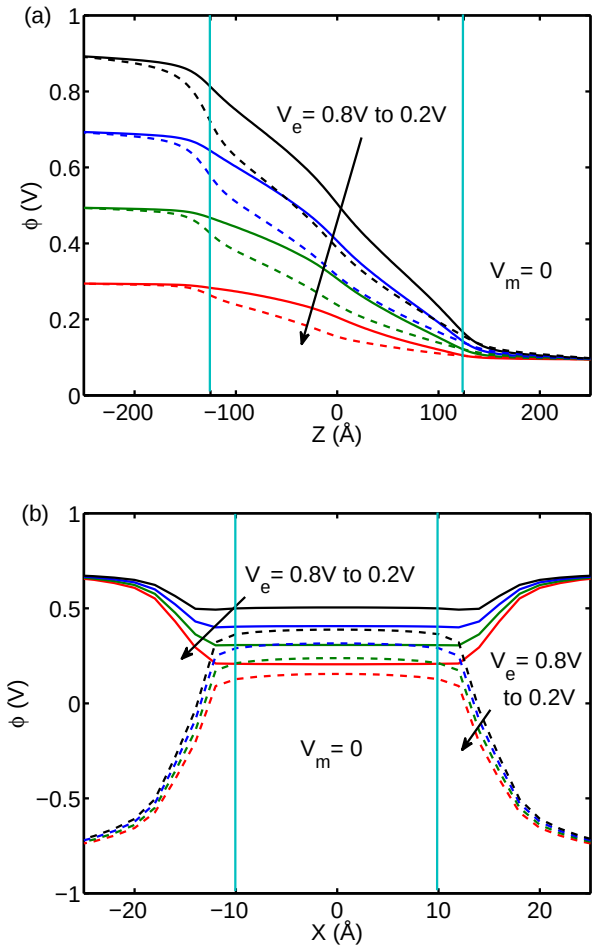

FIG. 2: (Color online)(a) Electrostatic potential profile $\phi(\mathbf{r})$ for n-Si membrane (solid lines) and p-Si membrane (dashed lines) through the center of the pore along the z-axis for electrolyte biases V_e = 0.2 V, 0.4 V, 0.6 V, and 0.8 V and V_m = 0 V. (b) Same as (a) but along the x-axis. Vertical lines indicate the boundaries for the membrane.

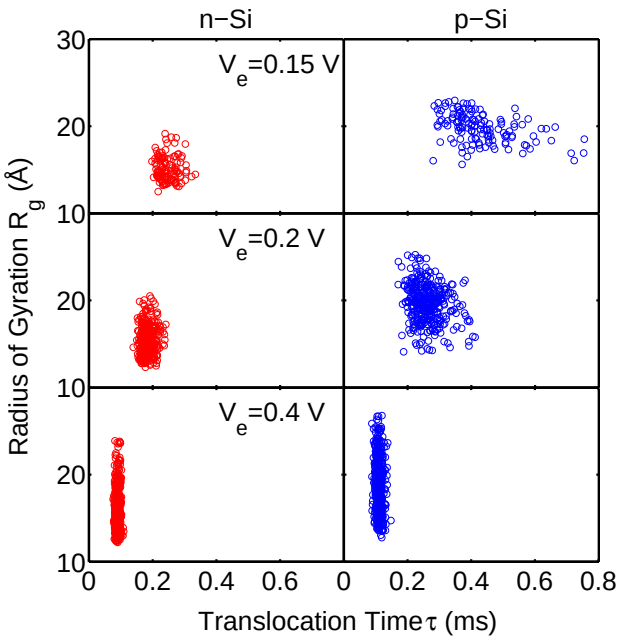

FIG. 3: (Color online) Scatter plots of the gyration radius R_g vs. translocation time τ for n-Si membrane (left) and for p-Si membrane (right) at various V_e given in plots. The data for V_e = 0.6 V and 0.8 V are not shown as they are similar to those at V_e = 0.4 V.

the directional translocation of the negatively charged biomolecule. As V_e decreases, the magnitude of electric field in this direction also decreases. This leads to a diminished value of the "driving" force resulting in a slower translocation process. This is later confirmed by larger recorded translocation times of the biomolecule (see Fig. 4a). Fig. 2b shows ϕ along the x-direction, perpendicular to the pore's axis. In this direction the potential is almost constant within the pore, particularly for the n-Si membrane. This suggests that the membrane has no effect on the electrolyte ion distribution within the pore under these conditions. Due to the difference in doping it is clear from Fig. 2 that the potentials of n-Si membrane are higher than those of the p-Si membrane.

The result of varying electric potentials (shown in Fig. 2) on DNA translocation is presented in Fig. 3. The scatter plots show the R_g values against the τ for each BD simulation. As V_e increases, the values of τ gradually become more concentrated at ~ 0.1 ms yet values of R_g become more widely distributed than at lower biases. This is because at lower electrolyte bias, the stochastic nature of DNA motion is more evident while increasing V_e leads to faster molecule translocation as well as its larger extension, particularly after passing the constriction. Note also, the R_g and τ values and their spread for p-Si membrane are larger for all V_e values. The reason is that in the p-Si membrane both doping and surface charge are negative, as opposed to n-Si membrane. In n-Si membrane the doping and surface charge have opposite signs and partially compensate each other, resulting in flatter potentials along the x-directions in Fig. 2b. Hence, the observed increase in both τ and R_g in a p-Si membrane is due to the decrease in the effective nanopore opening that further restricts movement of DNA[14].

The average values with standard deviations (error bars) of the translocation time $\langle\tau\rangle$ and the gyration radius $\langle R_g\rangle$ both extracted from the scatter plots in Fig. 3 are presented in Fig. 4. The average values and standard deviations of $\langle\tau\rangle$ ($\langle R_g\rangle$) are calculated using the collected data and basic statistical formulas for computation of the average and standard deviation.

The average translocation time increases with lowering of the electrolyte bias, as expected. A direct correlation between V_e and τ can be found using a simple drift model where the driving force from the electrolyte bias qV_e is balanced by the viscous drag force $\xi v \sim \xi(L/\tau)$, where L is the ssDNA length, resulting in $\langle\tau\rangle \sim V_e^{-1}$. Based

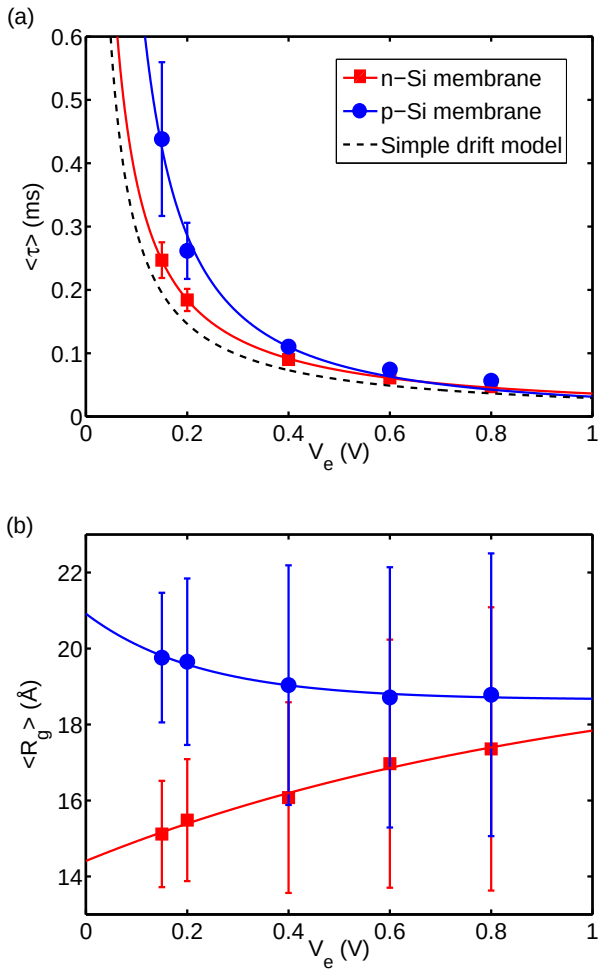

FIG. 4: (Color online)(a) Average translocation time $\langle\tau\rangle$ (with error bars) vs. electrolyte bias V_e for p-Si and n-Si membranes. The solid lines are results of fit using $\langle\tau\rangle \sim V_e^{-\alpha}$. Dashed line shows result of a simple drift model. (b) Average gyration radius $\langle R_g\rangle$ (with error bars) vs. electrolyte bias V_e for p-Si and n-Si membranes. The best-fit model used is $\langle R_g\rangle = R_0 \pm R_1 \exp[-\beta e V_e/k_B T]$ where for $n(p)$-Si membrane $R_0 = 19.86$ (18.65) Å, $R_1 = 5.45$ (2.26) Å and $\beta = 0.026$ (0.115).

on this concept, we fit the dependence of $\langle\tau\rangle$ on V_e in Fig. 4a to $\langle\tau\rangle \sim V_e^{-\alpha}$ with α being a variational parameter. Both n-Si and p-Si membranes show the same general trend in dependency of $\langle\tau\rangle$ on V_e with similar values of $\alpha = 1.13(1.41)$ for n-Si (p-Si) membrane. We also observe that as V_e increases, the difference in $\langle\tau\rangle$ between n-Si and p-Si membrane decreases, and at $V_e = 0.8$ V it reaches the value of ~ 0.08 ms which corresponds to translocation speed of ~ 2 μs/base. This is easily explained by the fact that as V_e becomes larger the doping of membrane has a lesser role in the biomolecule motion.

Larger values of τ at low V_e for p-Si membrane (larger α) can also be explained by the decreased effective diameter of the pore resulting in a larger entropy barrier[38] at the constriction leading to longer time for the ssDNA to permeate through the membrane. Since longer translocation times are important for practical applications, the case of small V_e is considered in detail in the following subsection.

In Fig. 4b we see that p-Si and n-Si membrane show different dependencies of $\langle R_g\rangle$ on V_e. Here we note that as V_e increases, $\langle R_g\rangle$ increases with V_e for n-Si membrane and $\langle R_g\rangle$ decreases with V_e for p-Si membrane. The increase (decrease) has its origin in the type of membrane doping involved. For n-Si membrane, the effect of the membrane surface charge is diminished which leads to faster relaxation and decreased R_g at small V_e. As for p-Si membrane, it pushes away negatively charged DNA towards the central axis of the nanopore, constricting its motion in a smaller effective pore radius and simultaneously extending it along z-direction (hence R_g is larger at low V_e). For both membranes, R_g approaches the same value of ~ 18 Å at $V_e \sim 1$ V where doping no longer plays a significant role and ssDNA motion is dominated by the external electrolyte bias.

B. Non-Zero Membrane Bias: $V_m \neq 0$

To further elucidate the effects of doping and applied membrane bias on the ssDNA translocation dynamics and show how these effects can be controlled, we performed additional simulations at $V_e = 0.15$ V and 0.20 V while varying -1.0 V$\leq V_m \leq 1.0$ V. Similar to Fig. 2, from Fig. 5 ($V_e = 0.15$ V) we can see that there is a monotonic variation of the potential along the z-axis of the pore. This potential is due to the applied V_e and $\phi(\mathbf{r})$ is larger for n-Si membrane than p-Si membrane at the same value of V_m (the potential profiles for $V_e = 0.20$ V are not shown due to similarity to those displayed in Fig. 5). Along the x-axis (Fig. 5b) the potential is not constant within the pore (note different vertical scales in Figs. 2a and 5b): for the p-Si membrane it decreases towards the surface in the range of the studied electrolyte biases while in the n-Si membrane it actually increases for positive V_e.

Looking at the dependency of $\langle\tau\rangle$ on V_m in Figs. 6(a & b) for two values of V_e, we observe different trends for n-Si and p-Si membranes. For p-Si membrane, $\langle\tau\rangle$ gradually increases as V_m decreases, with the largest $\langle\tau\rangle$ recorded for p-Si membrane at $V_e = 0.15$ V and $V_m = -1.0$ V being 0.75 ms. This corresponds to translocation speed of $\sim$ 17 μs/base (Fig. 6a). This increase is expected, considering the potential variation within the pore in the x-direction (see Fig. 5b). As seen in Fig. 5b, the potential decreases away from the center faster when V_m is lowered. This results in a stronger repulsion of the negatively charged biomolecule from the surface of the pore and a smaller effective pore diameter (similarly to the above discussion in Section III A but to a larger degree), consequently increasing potential and entropy barriers at the pore's entrance and constriction which leads to the increased translocation time. For $V_e = 0.20$ V, ss-

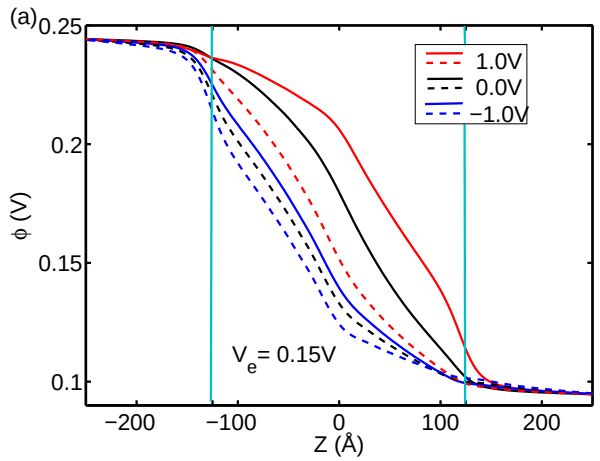

FIG. 5: (Color online) Electrostatic potential $\phi(\mathbf{r})$ through the center of the pore along the z-axis and x-axis (see Fig. 1) for $V_e = 0.15$ V at various membrane biases V_m for n-Si (solid lines) and p-Si (dashed lines) membranes. The inset in (b) shows the enlarged section corresponding to -10 Å$\leq x \leq$ 10 Å. The two vertical lines indicate the membrane boundaries.

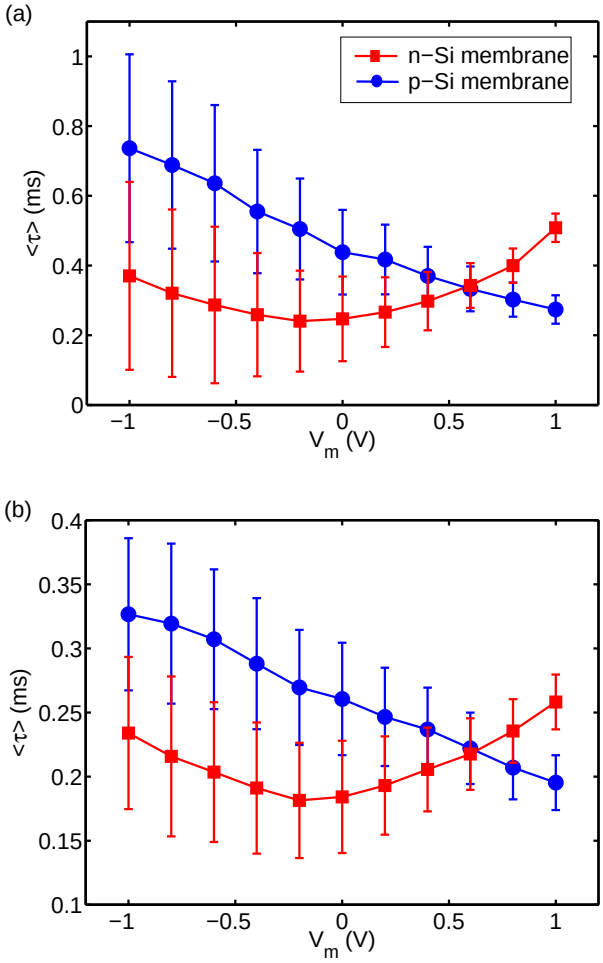

FIG. 6: (Color online) Average translocation time $\langle\tau\rangle$ with error bars as a function of the membrane bias V_m for p-Si and n-Si membrane at (a) $V_e = 0.15$ V and (b) $V_e = 0.20$ V.

DNA moves faster (Fig. 6b) but the same trend in $\langle\tau\rangle$ vs. V_m persists.

For n-Si membrane, the dependency of $\langle\tau\rangle$ is more complicated. The smallest $\langle\tau\rangle$ is recorded for V_m around 0 V and gradually increases with applied $|V_m|$. When $V_m \sim 0$ V, the potential across the pore is almost constant (see inset in Fig. 5b) indicating very little interference from ϕ on the biomolecule translocation. For the negative values of V_m, the trend is similar to that of p-Si membrane and can be explained in the same manner since they have very similar potential variations within the pore (Fig. 5b). For the positive values of V_m, the increase in $\langle\tau\rangle$ as V_m increases is due to the attraction of DNA to the surface inside the pore (the biomolecule is attracted to the surface). This is a result of the potential increasing away from the center rather than decreasing as in negative values of V_m. Such an increase in $\langle\tau\rangle$ for $V_m > 0$ was also recently experimentally observed in the n-doped Si membrane[39].

This explanation of tendencies in translocation time behavior is confirmed by changes in $\langle R_g\rangle$ vs. V_m depicted in Figs. 7(a & b) which are qualitatively similar for both membranes. At large and negative V_m, strong lateral electric field constricts and extends ssDNA so that its length increases. When V_m becomes positive, the lateral electric field either becomes small or changes its direction altogether resulting in a more "relaxed" dynamics of DNA translocation with a smaller overall biomolecule extension. Note that the large difference in $\langle R_g\rangle$ values for $V_m \gtrsim 0$ between n-Si and p-Si membranes ($\langle R_g\rangle$ larger for p-Si membrane) is due to the larger overall negative charge in p-Si membrane repelling and constricting the DNA which requires larger membrane biases to overcome this influence.

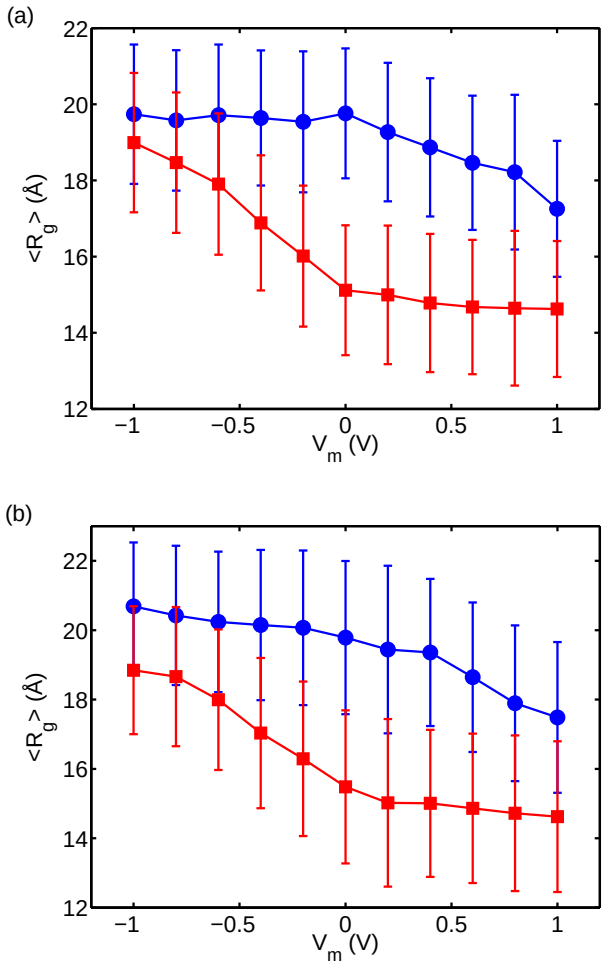

FIG. 7: (Color online) Same as in Fig. 6 but for gyration radius $\langle R_g \rangle$.

IV. CONCLUSION

In this work, we investigated the motion of the ss-DNA through a double-conical nanopore in a doped, nanometer-thin Si membrane using a modeled system. We considered influences of both p- and n-doping, applied electrolyte, and membrane biases on DNA dynamics. To describe the biomolecule and its movement, we utilized the BD model while the electric potential was computed from the self-consistent PNP model.

We found that at higher applied electrolyte biases both n-Si and p-Si membrane show very similar behavior and the effects of doping are not pronounced. At lower electrolyte biases, such as 0.15 and 0.20 V, the effects of doping become more prominent, with p-Si membrane exhibiting longer translocation time and greater DNA extension.

For both membranes, the relation between translocation time and electrolyte bias, V_e, is $\sim 1/V_e$ with the p-Si membrane showing larger deviation. We attribute this deviation as well as longer translocation time and larger biomolecule extension to the decrease in effective pore diameter caused by the negative charges in/and on the p-Si membrane. Thus DNA passage is more constricted through p-Si membrane than through n-Si membrane. The translocation dynamics of DNA can be further controlled and tuned by application of bias to the membrane. We find that the biomolecule translocation time can be control by the applied membrane bias in the interval from 2 μs/base to 17 μs/base. To achieve a greater degree of control over the DNA translocation time, semiconductor membranes with multiple layers may also be used[9,14].

At present, the obvious limitations of our model are the absence of the electro-osmotic effects and the lack of a self-consistency between the biomolecule motion and the open pore PNP calculations. These can be justified by the small size of our pores where effects of the membrane are the dominant factor. However, for larger pore sizes, the above issues should be addressed as, for example, electrophoretic flow could become important in discussing the DNA dynamics[40].

Acknowledgments

This work was supported by the NSF grant CBET-1119446 and by the XSEDE awards for computational resources TG-PHY110023 and TG-TRA120010. We are grateful to Zachery Hulings for the critical reading of the manuscript.

[1] J. Kasianowicz, J. Robertson, E. Chan, and V. Stanford, Ann. Rev. Analyt. Chem. **1**, 737 (2008).
[2] J. Kasianowicz, E. Brandin, D. Branton, and D. Deamer, Proc. Nat. Ac. Sci. USA **93**, 13770 (1996).
[3] R. M. M. Smeets, U. F. Keyser, D. Krapf, M. Y. Wu, N. H. Dekker, and C. Dekker, Nano Lett. **6**, 89 (2006).
[4] M. Wanunu, J. Sutin, B. McNally, A. Chow, and A. Meller, Biophys. J. **95**, 4716 (2008).
[5] J. Li, M. Gershow, D. Stein, E. Brandin, and J. Golovchenko, Nature Mat. **2**, 611 (2003).
[6] D. Fologea, M. Gershow, B. Ledden, D. McNabb, J. Golovchenko, and J. Li, Nano Lett. **5**, 1905 (2005).
[7] S. Howorka and Z. Siwy, Chem. Soc. Rev. **38**, 2360 (2009).
[8] M. E. Gracheva, A. Xiong, A. Aksimentiev, K. Schulten, G. Timp, and J.-P. Leburton, Nanotechnology **17**, 622 (2006).
[9] M. E. Gracheva and J.-P. Leburton, Nanotechnology **18**, 145704 (2007).
[10] M. E. Gracheva, J. Vidal, and J.-P. Leburton, Nano Lett. **7**, 1717 (2007), ISSN 1530-6984.
[11] K.-Y. Chun, S. Mafe, P. Ramirez, and P. Stroeve, Chem. Phys. Lett. **418**, 561 (2006).
[12] R. Karnik, K. Castelino, and A. Majumdar, Appl. Phys. Lett. **88**, 1 (2006).

[13] Z. Jiang and D. Stein, Phys. Rev. E **83**, 031203 (2011).
[14] D. Melnikov, J.-P. Leburton, and M. Gracheva, Nanotechnology **23**, 25501 (2012).
[15] J. Li, D. Stein, C. McMullan, D. Branton, M. Aziz, and J. Golovchenko, Nature **412**, 166 (2001).
[16] M. Wanunu, T. Dadosh, V. Ray, J. Jin, L. McReynolds, and M. Drndić, Nature Nanotech. **5**, 807 (2010).
[17] A. Meller, J. Phys. Cond. Matt. **15**, R581 (2003).
[18] D. Fologea, J. Uplinger, B. Thomas, D. McNabb, and J. Li, Nano Lett. **5**, 1734 (2005).
[19] M. Akeson, D. Branton, J. Kasianowicz, E. Brandin, and D. Deamer, Biophys. J. **77**, 3227 (1999).
[20] A. Meller, L. Nivon, E. Brandin, J. Golovchenko, and D. Branton, Proc. Nat. Ac. Sci. USA **97**, 1079 (2000).
[21] M. E. Gracheva, A. Aksimentiev, and J.-P. Leburton, Nanotechnology **17**, 3160 (2006).
[22] D. Deamer and D. Branton, Acc. Chem. Res. **35**, 817 (2002).
[23] U. Keyser, J. Royal Soc. Interface **8**, 1369 (2010).
[24] A. Nikolaev and M. Gracheva, Nanotechnology **22**, 165202 (2011).
[25] S. H. Chung and B. Corry, Soft Matter **1**, 417 (2005).
[26] P. Graf, A. Nitzan, M. Kurnikova, and R. Coalson, J. Phys. Chem. B **104**, 12324 (2000).
[27] F. Lanzerath, D. B. and H. Trinkaus, M. Goryll, S. Mantl, J. Knoch, U. Breuer, W. Skorupa, and B. Ghyselen, J. Appl. Phys. **104**, 044908 (2008).
[28] S. M. Sze, *Physics of Semiconductor Devices* (John Wiley & Sons Ltd., New York, 1981).
[29] J. Vidal, M. E. Gracheva, and J.-P. Leburton, Nanoscale Res. Lett. **2**, 61 (2007).
[30] M. E. Gracheva, D. V. Melnikov, and J.-P. Leburton, ACS Nano **2**, 2349 (2008).
[31] A. Nikolaev and M. Gracheva, Nanotechnology **22**, 165202 (2011).
[32] M. Muthukumar and C. Y. Kong, Proc. Nat. Ac. Sci. USA **103**, 5273 (2006).
[33] N. Watari, M. Doi, and R. Larson, Phys. Rev. E **78**, 01180111 (2008).
[34] M. Kenward and K. D. Dorfman, J. Chem. Phys. **130**, 095101 (2009).
[35] M. Fyta, S. Melchionna, M. Bernaschi, E. Kaxiras, and S. Succi, J. Stat. Mech. **6**, 06009 (2009).
[36] A. Bhattacharya and K. Binder, Phys. Rev. E **81**, 041804 (2010).
[37] S. Smith, Y. Cui, and C. Bustamante, Science **271**, 795 (1996).
[38] M. Muthukumar, Ann. Rev. Biophys. Biomol. Struct. **36**, 435 (2007).
[39] P. Yen, C. Wang, G. Hwang, and Y. Chou, Rev. Sci. Instrum. **83**, 034301 (2012).
[40] B. Luan and A. Aksimentiev, Phys. Rev. E **78**, 021912 (2008).